



HAL
open science

Rock mass behavior in deep mines: in situ monitoring and numerical modelling

Francesca de Santis, Vincent Renaud, Isabelle Contrucci, Yann Gunzburger,
Pascal Bernard

► **To cite this version:**

Francesca de Santis, Vincent Renaud, Isabelle Contrucci, Yann Gunzburger, Pascal Bernard. Rock mass behavior in deep mines: in situ monitoring and numerical modelling. 14. International congress of rock mechanics (ISRM 2019), Sep 2019, Foz do Iguassu, Brazil. ineris-03237766

HAL Id: ineris-03237766

<https://ineris.hal.science/ineris-03237766>

Submitted on 26 May 2021

HAL is a multi-disciplinary open access archive for the deposit and dissemination of scientific research documents, whether they are published or not. The documents may come from teaching and research institutions in France or abroad, or from public or private research centers.

L'archive ouverte pluridisciplinaire **HAL**, est destinée au dépôt et à la diffusion de documents scientifiques de niveau recherche, publiés ou non, émanant des établissements d'enseignement et de recherche français ou étrangers, des laboratoires publics ou privés.

Rock mass behavior in deep mines: in situ monitoring and numerical modelling

F. De Santis, V. Renaud & I. Contrucci

Ineris, Nancy, France

Y. Gunzburger

GeoRessources - Université de Lorraine - CNRS, Nancy, France

P. Bernard

IPGP, Paris, France

ABSTRACT: With the aim of better understanding the mechanical behavior of rocks solicited by underground excavations, the rock mass response to mining was studied based on a comprehensive approach. For this purpose, a deep area of the metal mine of Garpenberg (Sweden) was instrumented with a geophysical and geotechnical monitoring network. In situ monitoring data were analyzed and interpreted considering the specific mining method and the local geological setting. In addition, an advanced 3D elasto-plastic numerical model of the mine was built to better understand the interactions between quasi-static stress changes due to mining and the generation of the induced seismicity. Results show a complex rock mass response, strongly influenced by mining and geological characteristics, both in term of seismic and aseismic phenomena. The case study of Garpenberg also highlights the strong potentiality of the proposed approach, which can help improving the seismic hazard assessment in deep mining operations.

1 INTRODUCTION

Excavations in underground mines induce perturbations of the in situ stress regime. The induced stresses cause seismic and aseismic deformations in the surrounding rock masses, which can both require significant efforts in term of rock mass stability and mining strategies, as well as threaten mine workers safety.

Seismic monitoring in underground mines is nowadays a common tool to assess the seismic hazard induced by mining and to prevent seismic risk. Similarly, numerical modelling techniques are widely used as an aid for decision making, for planning long-term mining strategies and for defining the optimal mining sequence. These two techniques, even if largely applied, are generally regarded as separated tools with distinct objectives.

This paper proposes to analyze the mechanical response of rock masses to mining based on a comprehensive approach, which considers geotechnical and geophysical data, along with 3D numerical modelling, and accounts for mining practices and the local geological setting.

With the aim of working in a real mine environment, the proposed methodology is applied to the underground hard-rock mine of Garpenberg (Sweden), operated by the Boliden mining company. In the framework of the European project *I²Mine*, the French National Institute for Industrial Environment and Risks (Ineris) instrumented a deep area of the Garpenberg mine with a monitoring network consisting of both seismic probes and geotechnical cells, for monitoring mining-induced seismicity and quasi-static strain changes in response to excavation. Boliden provides information about mine production and blasting operations, which are integrated in the Ineris web platform *e.cenaris* together with geophysical and geotechnical data. This rich data flow in constant update constitutes a unique opportunity for studying the rock mass behavior at Garpenberg mine, with the more global objective of improving seismic hazard assessment in deep mining operations.

2 STUDY AREA AND MONITORING NETWORK

Garpenberg mine is characterized by several polymetallic sulphide deposits, of which Lappberget is the deepest and the largest orebody, with a whole vertical extension between 435 m and 1600 m below ground surface. The study area of this article (Fig. 1) is the block 1250 of Lappberget orebody, which ranges between 1108 m and 1257 m depth.

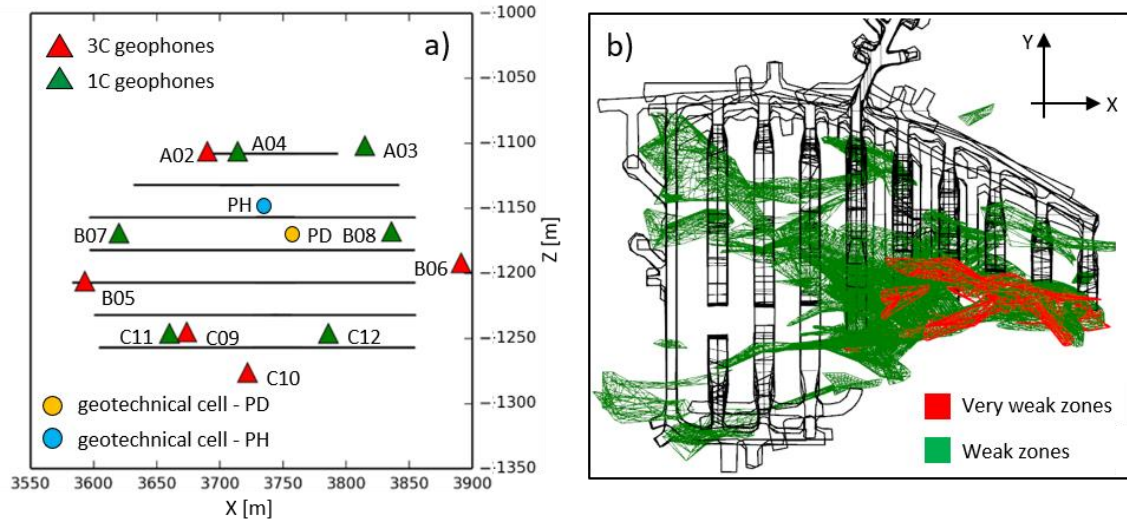


Figure 1. Monitoring network (a) and geological setting (b).

Lappberget is an almost vertical orebody, mainly hosted in a limestone-dolomite unit (Ahmadi et al. 2013). All along the orebody, mine geologists have identified the presence of some weak and very weak zones (Fig. 1b). These areas are mainly characterized by schists with large amounts of talc and other types of soft minerals. As illustrated in Figure 1b, weak and very weak zones are mostly deployed in the eastern part of the study area making it extremely heterogeneous.

Ore production in block 1250 is performed by the sublevel stoping method. This technique consists in charging and then blasting the orebody between two consecutive levels, creating voids of about 25 m size in the vertical direction, which are called (sub-) stopes (Fig. 2a). Once blasted and mucked out, stopes are backfilled with paste. Generally, more than one blast is needed for producing the orebody along the entire length of a drift (Fig. 2b).

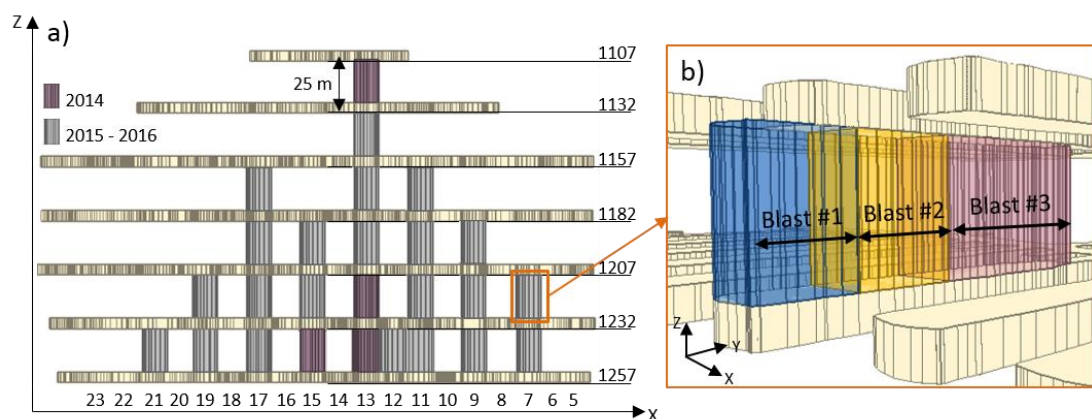


Figure 2. Mining method and sequencing. (a) Vertical profile showing all sub-stopes extracted between 2014 and 2016. Numbers at the bottom indicate stopes' names, while numbers on the right refer to mine's levels. (b) 3D view between two consecutive levels, showing the blast design along the length of a drift.

The mining method is based on a sequence of alternated primary and secondary stopes. Primary stopes are named by odd numbers, while even numbers indicate secondary stopes (Fig. 2a). As

the name suggests, primary stopes are the first to be blasted, while secondary stopes, located in between are excavated only when the adjacent primaries have been mined and backfilled.

This paper focuses on production performed in block 1250 between February 2015 and December 2016. During this period, 52 sub-stopes have been excavated in block 1250 and the stope 13 was completely mined-out, from the bottom to the top of the block. Stope 13 was excavated following a coupled bottom-up and top-down sequence, leaving one sub-stope in the central area of the column which was extracted last (sub-stope between levels 1157 and 1182 in Fig. 2a).

At the end of 2014, block 1250 of Lappberget was instrumented with a monitoring network (Fig. 1a) installed by Ineris (Tonnellier et al. 2016). The network consists of 2 CSIRO (PD and PH) strain cells and 11 SYTMIS seismic sensors.

For a detailed description of the network, of the methodology used for seismic events localization and seismic source parameter estimation, the reader is referred to De Santis et al. (2018) and De Santis (2019).

3 GEOMECHANICAL NUMERICAL MODELLING

In order to evaluate stresses induced by mining in block 1250, a large-scale, densely-meshed, 3D continuous numerical model has been set up and run using a finite difference code. The model simulates the exact mining sequence, with a total of 52 extracted sub-stopes, simulated in 52 model steps.

3.1 Model geometry and meshing

The numerical model proposed in this article was built in order to reconstruct, as accurately as possible, the geometry of excavations and the geological setting of block 1250, which constitutes our area of interest. Elements which were reconstructed are the ore volume, the weak and very weak zones, as well as mine galleries and stopes within block 1250 (close-up of Fig. 3). In addition, mined-out areas above block 1250 were as well considered in the model (see Upper levels in Fig. 3).

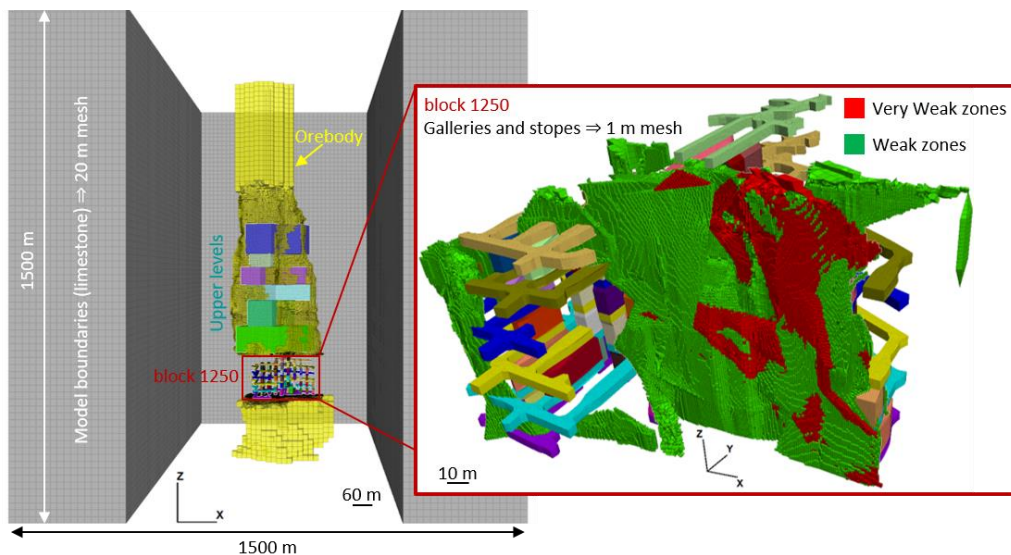


Figure 3. Geometry and meshing of the numerical model. The orebody is reported in yellow, while gray areas are assigned to the limestone. In the close-up weak and very weak zones are reported in green and red, respectively.

Model boundaries were designed far enough from excavations to avoid boundary effects. Model mesh was built at varying degrees of details, with a high resolution (*i.e.* a small size) within the area of interest (block 1250) and being coarser (*i.e.* larger) further away. The final 3D volumetric mesh consists of about 13.3 million elements.

3.2 Initial and boundary conditions

Null normal displacement conditions were used. The virgin stress state adopted in the proposed numerical model is the one retrieved by Souley et al. (2018), which was back-computed by numerical modelling based on stress measurements carried out in December 2014 at -1155 m. At this depth, the retrieved virgin stress state is as follow: $\sigma_1 = 47.3$ MPa, $\sigma_2 = 44.4$ MPa and $\sigma_3 = 34.3$ MPa. It was obtained by imposing that the vertical principal stress equals the overburden weight. Orientation of the stress state assumes that the major principal stress is parallel to mine drifts (along the Y direction of the mine) and that the intermediate principal stress is oriented along the X direction of the mine.

3.3 Rock mass properties and constitutive laws

To determine the rock-mass geomechanical parameters, the unconfined compressive strength (UCS) of the intact rock, the Hoek-Brown material constant (m_i) and the Geological Strength Index (GSI) were selected for each considered geological unit, based on rock mass types, structures and discontinuities. The elastic material properties, namely the Young modulus (E) and the Poisson ratio (ν), were determined choosing mean values from biaxial tests performed on rock samples and pastefill (Tab. 1). Finally, the UCS and m_i values of the intact rock and the GSI values of the rock mass were used to calculate the Hoek-Brown constants m and s based on the following empirical relations (Hoek & Brown 1997):

$$m = m_i \exp\left(\frac{GSI - 100}{28}\right) \quad (1)$$

$$s = \exp\left(\frac{GSI - 100}{9}\right) \quad (2)$$

The geomechanical parameters are listed in Table 1.

Table 1. Geomechanical parameters retained for numerical modelling.

Material	UCS	m_i	GSI	E	ν	m	s
Units	MPa	-	-	GPa	-	-	-
Ore	188	20	80	66	0.2	10	0.112
Limestone	110	20	80	57	0.18	10	0.112
Weak	30	9	38	20	0.3	1.0	0.001
Very weak	10	9	25	2	0.4	0.63	0.00024
Pastefill	-	-	-	0.5	0.2	-	-

Assuming that neither thermal, nor hydraulic effects occur, rock masses in the proposed numerical model were modelled assuming purely mechanical constitutive laws. More precisely, limestone, weak zones and very weak zones were modelled considering a perfectly plastic behavior with a parabolic failure criterion (Hoek & Brown 1997). While, for the ore we assumed an elastoplastic behavior which considers the brittle-ductile transition in the post-peak phase (Souley et al. 2018). Finally, a linear elastic behavior was assumed for the paste.

4 RESULTS

4.1 Seismic activity and slope's production

During the analyzed period, more than 750 microseismic events were located around mine galleries in block 1250, with moment magnitudes ranging between -2 and 0.8. Six major seismic sequences were observed (indicated by vertical lines in Fig. 4a), which correspond to a strong increase of the seismic rate. Apart from one sequence (sequence 4 in Fig. 4a), all the others occurred in coincidence with production blasts. However, the intensity of the induced seismicity is not proportional to the blasted volume (dots at the top of Fig. 4a).

When looking at the position of the five blasted sub-stopes (red blocks in Fig. 4b) which resulted in the intensification of the seismic rate, it is interesting to observe that these are all related to production in Stope 13 and particularly to its final exploitation steps. This observation indicates that mine production has a primary role in the generation of the seismic activity, but seismicity is more related to blast positions (i.e. mine sequencing) than to the blasted volume.

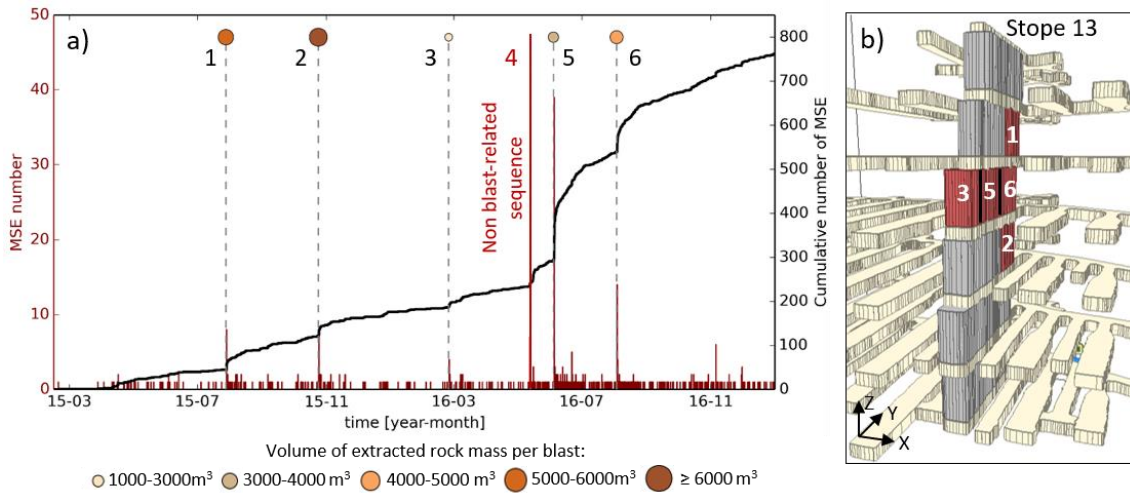


Figure 4. Seismic activity and mine production.

The spatial distribution of seismicity (see Fig. 5 in De Santis et al. 2018) is characterized by two main clusters: the central cluster (CC), located near Stope 13 in the main production area, and the right cluster (RC) located in the eastern part of the mine, where the major weak geological zone is situated. If CC seismicity can be seen as a direct response of the rock mass to local blasting, the intense seismicity of the RC cannot be explained by the small production performed in this region. Microseismic events in RC were remotely triggered by the two last production blasts performed in Stope 13 (5 and 6 in Fig. 4b), which had the potential to induce seismicity at more than 70 m distance from the production area.

As already pointed out by De Santis et al. (2018), seismic source parameters indicate that CC and RC are characterized by events with significantly different dynamics. This can be explained considering the strong heterogeneity of the eastern part of the mine. Geological heterogeneities strongly influence fracture propagation within the RC, due to the presence of the weak lenses at direct contact with the breaking stiff rock mass. Consequently, RC events are characterized by smaller fracture dimensions (*i.e.* source radii) than the events nucleated within the CC area. Source radii were calculated from the corner frequency of microseismic events and considering the circular source model of Madariaga (1976). In addition, due to inhomogeneous geological properties, the local stress field is heterogeneously distributed in the RC, with high stress levels within the stiff rocks surrounded by weak geological areas.

4.2 Geotechnical measurements analysis

The analysis of strain measurements retrieved from CSIRO cells shows that the rock mass was solicited by many production blasts. During the analyzed period, 20 strain shifts were observed immediately after nearby production. Of the total detected shifts, 13 are the more significant in terms of intensity, with maximum strains jumps ranging between 20 $\mu\text{m}/\text{m}$ to more than 2000 $\mu\text{m}/\text{m}$.

Considering the large number of recorded strain shifts with respect to the small number of observed seismic sequences, it appears evident that most of the stopes were extracted inducing aseismic deformations in the surrounding rock mass, but no seismicity.

Moreover, for most of the observed shifts, the measured strain rates do not return quickly to the steady state after the sudden increase induced by blasting. Therefore, induced strains are long-lasting in time, suggesting that a mechanism of creep occurs in response to blasting. An aseismic

creep phenomenon could explain the occurrence of a seismic sequence not directly triggered by blasting (sequence 4), as well as the delayed reactivations of seismic rate observed for the analyzed seismic sequences. Indeed, under particular configurations, silent creep induced by blasting in aseismic regions (e.g. weakness zones) has the potential to gradually load adjacent seismic asperities, bringing them to the rupture and triggering seismicity. However, further analysis will be needed in future studies to deeper investigate this aspect.

4.3 Numerical modelling results

Model results are presented in Figure 5a and 5b in the form of deviatoric stress (q) contours, for two different model steps. The deviatoric stress, or Von Mises equivalent stress, is written as follow:

$$q = \sqrt{\frac{1}{2} \left[(\sigma_1 - \sigma_2)^2 + (\sigma_1 - \sigma_3)^2 + (\sigma_3 - \sigma_2)^2 \right]} \quad (3)$$

where σ_1 , σ_2 and σ_3 , are the major, the intermediate and the minor principal stress, respectively.

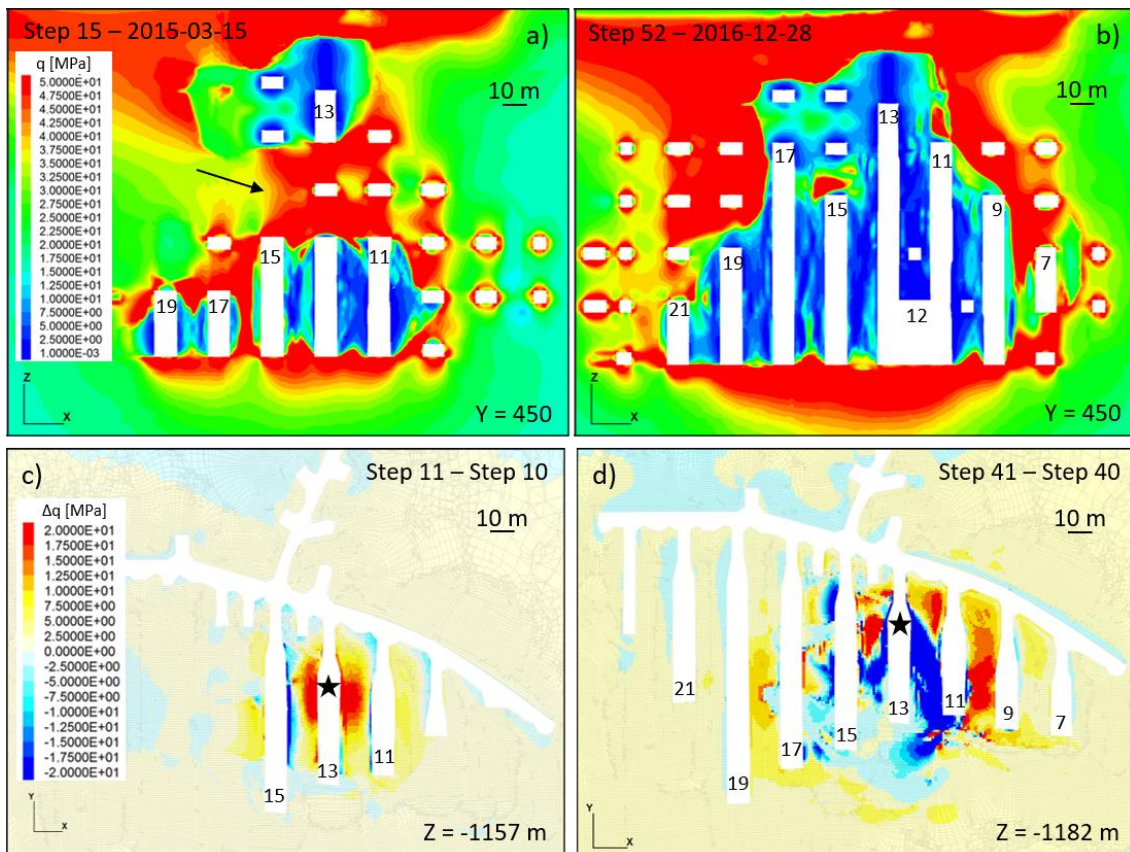


Figure 5. (a, b) Contour maps of deviatoric stress along a vertical section for model steps 15 (a) and 52 (b). (c, d) Difference in deviatoric stress between subsequent model steps along a horizontal section. Numbers in the figures indicate stopes' names.

Excavations have the effect of destressing secondary stopes adjacent to mined-out primary ones (Fig. 5a and 5b). Consequently, higher stresses are gradually transferred to the sides of block 1250. As the volume of extracted rock increases, the destressed zone become wider (Fig. 5b).

Figure 5a also highlights the effect on stress redistribution due to the chosen mining sequence in Stope 13. Indeed, the coupled bottom-up and top-down sequence results in two distinct zones characterized by lower stresses around mined volumes, interrupted by an area (indicated by an arrow in Fig. 5a), where deviatoric stresses are higher. In this central zone, the deviatoric stress retrieved by modelling reaches more than 60 MPa, immediately prior the complete excavation of

Stope 13, which means an increase of more than 5 times with respect to its initial value (equals to 11.6 MPa at the average depth of -1182 m).

As the excavation progresses, areas influenced by blasting are gradually moved further away from production zone. This is visible in Figure 5c and 5d, which reports the variation in deviatoric stress between consecutive model steps. At Step 11 (Fig. 5c), when only small volumes of rock have been extracted, the production blast (indicated by a star) has a purely local effect. Induced stresses appear to be mostly redistributed in zones near the excavation, particularly in the adjacent secondary stopes. Overall the blast appears having a radius of influence of about 15 m around the excavation. As the production progresses within Stope 13, the zone influenced by blasting is progressively enlarged and stresses are transferred further away from the production area (Fig. 5d).

This trend agrees with the recorded seismic activity, with the occurrence of seismic events at greater distance from blasted areas in coincidence with the final production stages of Stope 13.

4.4 Analysis of seismic active regions in the numerical model

To deeper analyze the rock mass response to mining, we selected sub-volumes within the whole area of interest of the numerical model (i.e. block 1250), identified by 10-m radius spheres centered at microseismic event hypocenters.

Figure 6 compares the mean values of deviatoric stress retrieved by numerical modelling within spheres located in the CC and RC (hereafter CC_M and RC_M), with the number of microseismic events recorded in these regions throughout the study period. Mean stresses within RC_M are gradually increasing, reaching 10 MPa difference at the end of the study period, while CC_M is characterized by smaller stress changes, with a maximum increase of about 2.6 MPa (Fig. 6a). Overall, mean stresses remain higher within CC_M . However, at the end of the analyzed period, mean stresses are comparable within these two regions of the mine due to the increase of stress state within RC_M and the concurrent stress decrease in CC_M .

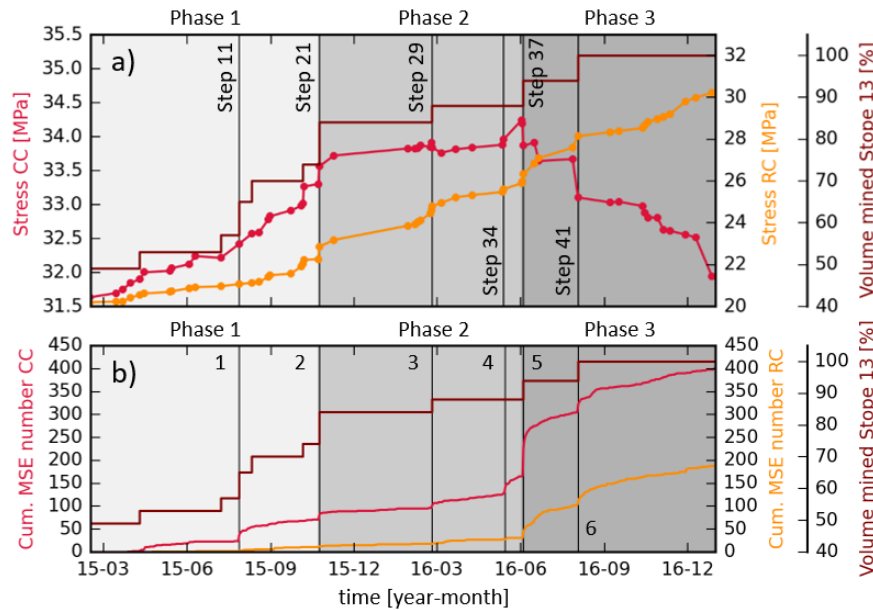


Figure 6. Mean values of deviatoric stress retrieved at each model step in CC_M and RC_M (a). Cumulative number of seismic events in CC and RC during the analyzed period (b).

Three distinct phases can be identified in Figure 6, which are marked with different background colors. At the beginning of the analyzed period and until Step 21 (Phase 1), CC_M and RC_M regions present similar rates of stress increase. Then, from Step 21 to Step 36 (Phase 2), stress remains almost constant within CC_M at the highest level, while it increases significantly in the RC_M . Finally, after Step 37 (Phase 3), in coincidence with the two last stages of Stope 13 exploitation, stress state in CC_M starts dropping dramatically until the end of the study period, while stresses within RC_M keep rising.

Phase 1 and 2 are characterized by very low levels of seismic activity within RC, while seismicity is punctually and locally enhanced in the CC, due to production in Stope 13 (Fig. 6b). Remote seismicity in RC occurs during Phase 3, in coincidence with the destressing of the rock mass in the major production area (i.e. CC). This indicates that the remote seismicity within RC is triggered when the CC is not anymore able to sustain additional loads and stresses are transferred to RC where, due to geological heterogeneities, local stresses are already at high levels.

5 CONCLUSION

In this paper a comprehensive approach for studying the mechanical behavior of rock mass solicited by underground excavations has been proposed. Results significantly enhanced our understanding of the rock mass response to mining, highlighting a complex behavior.

At first, geophysical data, analyzed considering mining method and geological characteristics, showed that seismicity is strongly related to the chosen mining sequence and to the local geological context. As a result, the seismic response to mining can have a local and short-term behavior, as well as being long-lasting over time and remote from excavations.

The analysis of geotechnical measurements highlighted the occurrence of aseismic phenomena and creep mechanisms in response to exploitation, which can be as well responsible for triggering seismicity. Further analysis will be needed in order to deeper investigate this aspect.

Numerical modelling results showed how the chosen mining sequence for Stope 13, with one column of stopes being exploited upward and downward simultaneously, leads to high stress concentrations in the remaining pillar. Moreover, the analysis of seismically active regions within numerical model allowed to better understand mechanisms which lead to trigger remote seismicity.

In conclusion, this work aims to give a first insight into a multi-parameter approach for the evaluation and the prevention of induced seismicity and related collapses in the context of deep underground mines. The correlation between geophysical and geotechnical measures, together with numerical modelling analysis, allows not only to have a better understanding of the rock mass response to mining, but it also highlights the complementarity of these methodologies. Their combination in a new integrated approach can significantly improve underground mine design, reducing straightforward limitations of geophysical data, geotechnical measures and numerical modelling, which appears evident when these instruments are considered separately.

REFERENCES

- Ahmadi, O., Juhlin, C., Malehmir, A. & Munck, M. 2013. High-resolution 2D seismic imaging and forward modeling of a polymetallic sulfide deposit at Garpenberg, central Sweden. *Geophysics* 78: B339-B350.
- De Santis, F., Contrucci, I., Kinscher, J., Bernard, P., Renaud, V. & Gunzburger, Y. 2018. Impact of geological heterogeneities on induced-seismicity in a deep sublevel stoping mine. *Pure and Applied Geophysics*: 1-21.
- De Santis, F. 2019. Rock mass mechanical behavior in deep mines: in situ monitoring and numerical modelling for improving seismic hazard assessment. PhD thesis, University of Lorraine.
- Hoek, E. & Brown, E.T. 1997. Practical estimates of rock mass strength. *International journal of rock mechanics and mining sciences* 34: 1165–1186.
- Madariaga, R. 1976. Dynamics of an expanding circular fault. *Bulletin of the Seismological Society of America* 66: 639-666.
- Souley, M., Renaud, V., Al Heib, M., Bouffier, C., Lahaie, F. & Nyström, A. 2018. Numerical investigation of the development of the excavation damaged zone around a deep polymetallic ore mine. *International Journal of Rock Mechanics and Mining Sciences* 106: 165–175.
- Tonnellier, A., Bouffier, C., Renaud, V., Bigarré, P., Mozaffari, S., Nyström, A. & Fjellström, P. 2016. Integrating microseismic and 3D stress monitoring with numerical modeling to improve ground hazard assessment. In: *8th International Symposium on Ground Support in Mining and Underground Construction; Proc. intern. symp., Luleå, 12-14 September 2016*.